Intracellular Ca^{2+} stores control in vivo neuronal hyperactivity in a mouse model of Alzheimer's disease

Chommanad Lerdkrai[a,1], Nithi Asavapanumas[a], Bianca Brawek[a], Yury Kovalchuk[a], Nima Mojtahedi[a], Maria Olmedillas del Moral[a], and Olga Garaschuk[a,2]

[a]Institute of Physiology, Department of Neurophysiology, Eberhard Karls University of Tübingen, 72074 Tübingen, Germany

Edited by Nicholas Spitzer, University of California, San Diego, La Jolla, CA, and approved December 26, 2017 (received for review August 15, 2017)

Neuronal hyperactivity is the emerging functional hallmark of Alzheimer's disease (AD) in both humans and different mouse models, mediating an impairment of memory and cognition. The mechanisms underlying neuronal hyperactivity remain, however, elusive. In vivo Ca^{2+} imaging of somatic, dendritic, and axonal activity patterns of cortical neurons revealed that both healthy aging and AD-related mutations augment neuronal hyperactivity. The AD-related enhancement occurred even without amyloid deposition and neuroinflammation, mainly due to presenilin-mediated dysfunction of intracellular Ca^{2+} stores in presynaptic boutons, likely causing more frequent activation of synaptic NMDA receptors. In mutant but not wild-type mice, store emptying reduced both the frequency and amplitude of presynaptic Ca^{2+} transients and, most importantly, normalized neuronal network activity. Postsynaptically, the store dysfunction was minor and largely restricted to hyperactive cells. These findings identify presynaptic Ca^{2+} stores as a key element controlling AD-related neuronal hyperactivity and as a target for disease-modifying treatments.

amyloidosis | synaptic impairment | axonal boutons | dendritic calcium stores | NMDA

Alzheimer's disease (AD) is a fatal neurodegenerative disorder causing progressive memory impairment and neurodegeneration, thus gradually destroying a person's ability to learn, to reason, to communicate, and to carry out daily activities. Most cases of the disease are sporadic, with advancing age being the major risk factor. A fraction of patients with AD, however, have an inherited form of the disease. Familial AD (FAD) is most often linked to mutations in the genes encoding amyloid precursor protein (APP) and presenilin 1 (PS1) and PS2. Around 90% of all identified FAD mutations (>200 mutations in total) are located on the PS genes (1, 2). Presenilins have γ-secretase–dependent and –independent activities. As a part of the γ-secretase complex, they catalyze the intramembranous cleavage of APP; γ-secretase–independently, they control neurotransmitter release and Ca^{2+} handling by the intracellular Ca^{2+} stores (3–5). To date, there is no effective drug therapy of AD. Available drugs provide only symptomatic benefits for a limited time, and many recent clinical trials, mostly directed against amyloid accumulation within the brain, failed to halt the progression of AD (6), prompting the researchers to look for alternative treatment strategies.

From the functional point of view, neuronal hyperactivity represents one of the emerging hallmarks of AD found in both humans and animal models of the disorder. Thus, neuronal hyperactivity is consistently found in individuals with amnestic mild cognitive impairment (aMCI), and its strength correlates with the severity of subsequent cognitive decline/conversion to a dementia diagnosis as well as with the extent of neuronal injury affecting AD-specific regions of the aMCI brain (7). Moreover, patients with sporadic as well as familiar forms of the disease, particularly those carrying a mutation in the presenilin genes, have a dramatically higher risk for developing seizures (reviewed in refs. 5, 8, 9). Subclinical epileptiform activity has also been observed in nondemented carriers of the apolipoprotein E4, a known genetic risk factor of sporadic AD, as well as in 42% of young (58- to 68-y-old) patients with the sporadic form of AD (10, 11). Moreover, some cases of episodic amnestic wandering, agitation, and disorientation in AD are associated with epileptiform activity and can be prevented by antiepileptic drugs (5, 10). Finally, an antiepileptic drug, levetiracetam, which selectively dampens neurotransmitter release under conditions of elevated firing, but not baseline neurotransmission, significantly improves cognition in patients with aMCI (7, 12).

Neuronal hyperactivity was found in the cortex and hippocampus of many different mouse models of AD, including awake or anesthetized hAPP-J20, APP/PSEN1dE9, Tg2576, 5xFAD, 3xTg-AD, APP/TTA-EC, APP/TTA-CaMKIIα, APP23, APP_{swe}/$PS1_{G384A}$, APPPS1, APP/PS1, and hAPPJ9/FYN transgenic mice (9, 13–18), and our previous work (14) directly visualized hyperactive cortical neurons in vivo. Despite its widespread nature, the cellular/molecular mechanisms underlying neuronal hyperactivity in AD remain unclear (9). The majority of studies pointed toward the synaptic origin of neuronal hyperactivity (13–15, 19); however, they differed in the proposed mechanisms. Busche et al. (15) and Keskin et al. (20) identified soluble Aβ oligomers as an important source of neuronal hyperactivity, whereas Verret et al. (19) attributed this phenomenon to an interneuron-specific defect in voltage-gated sodium channel subunit Nav1.1. Furthermore, accumulating in vitro data suggest that intracellular Ca^{2+} stores also play a role in controlling the efficacy of synaptic transmission

Significance

Although both patients with Alzheimer's disease (AD) and mouse models of the disease suffer from a profound neuronal hyperactivity mediating an impairment of memory and cognition, the underlying mechanisms remain elusive. Here, we show that neuronal hyperactivity is a hallmark of healthy aging but is further aggravated by AD-related mutations in presenilin 1 protein. AD-mediated enhancement of neuronal hyperactivity occurred even in the absence of amyloid plaques and neuroinflammation, mainly due to a presenilin-mediated dysfunction of intracellular Ca^{2+} stores in presynaptic boutons, likely causing more frequent activation of synaptic NMDA receptors. Emptying the stores normalized neuronal network activity in mutant mice, thus identifying presynaptic Ca^{2+} stores as a key element controlling AD-related neuronal hyperactivity and as a target for disease-modifying treatments.

Author contributions: C.L., B.B., and O.G. designed research; C.L., N.A., B.B., Y.K., and M.O.d.M. performed research; C.L., N.A., B.B., Y.K., N.M., and M.O.d.M. analyzed data; and O.G. wrote the paper.

The authors declare no conflict of interest.

This article is a PNAS Direct Submission.

[1]Present address: Department of Physiology, Faculty of Veterinary Medicine, Kasetsart University, Bangkok, Thailand.

[2]To whom correspondence should be addressed. Email: olga.garaschuk@uni-tuebingen.de.

This article contains supporting information online at www.pnas.org/lookup/suppl/doi:10.1073/pnas.1714409115/-/DCSupplemental.

(3, 21–24), but in vivo functional properties of the intracellular Ca^{2+} stores, as well as their contribution to AD-related neuronal hyperactivity, remain unknown.

In the present study, we combined somatic, dendritic, and axonal in vivo Ca^{2+} imaging with targeted pharmacological treatments of layer 2/3 cortical neurons to ask following specific questions. Is neuronal hyperactivity a general sign of aging or a selective feature of AD-related pathology? Do intracellular Ca^{2+} stores contribute to neuronal hyperactivity in vivo? If the answer is "yes," which cellular/molecular mechanisms are involved?

Results

Both Aging and Ongoing Amyloid Deposition Enhance Neuronal Hyperactivity. To answer the above questions, we first analyzed the ongoing spontaneous activity of layer 2/3 cortical neurons in wild-type (WT) mice and in a mouse model of AD [APP_{swe}/$PS1_{G384A}$ mice (14), hereafter referred to as "AD mice"] by means of multicell bolus loading and in vivo Ca^{2+} imaging techniques (25, 26). As was reported previously (27), a Ca^{2+} indicator dye, Oregon Green BAPTA-1 (OGB-1) AM, labels not only neurons and astrocytes (Fig. 1 *A* and *B*, *Left*) but also amyloid plaques (Fig. 1*B*, *Left*), enabling simultaneous monitoring of different elements of the brain parenchyma.

At the age studied (10–14 mo), layer 2/3 neurons in both WT and AD mice showed spontaneous Ca^{2+} transients at frequencies typical for silent (0–0.25 transients per minute), normal (0.26–4 transients per minute), and hyperactive (>4 transients per minute) cells (14) (Fig. 1 *A* and *B*). Our data revealed a surprisingly high fraction of hyperactive cells in 10- to 14-mo-old WT mice (Fig. 1*C*), comparable to the fraction of hyperactive cells in 6- to 10-mo-old AD mice (14). In 10- to 14-mo-old AD mice, this fraction was even higher, amounting to 38% of the entire neuronal population (Fig. 1 *C*–*E*). The fraction of silent cells was smaller in 10- to 14-mo-old mice compared with 6- to 10-mo-old mice (compare figure 1C with figure 1D in ref. 14), suggesting that, in reality, neuronal hyperactivity is even higher but is counteracted by mechanisms leading to neuronal silencing. Consistently, the overall distribution of the frequencies of neuronal Ca^{2+} transients was significantly shifted to the right in AD mice compared with WT mice (Fig. 1*E*). At the same time, we did not observe any significant difference in the amplitudes of spontaneous Ca^{2+} transients between AD and WT mice (n = 121 cells in five WT mice and n = 135 cells in five AD mice; Student's t test: $t_8 = 1.14$, $P = 0.29$).

Altogether, these data show that neuronal hyperactivity substantially increases with age in both WT and AD mice. In 10- to 14-mo-old AD mice, it represents the most prominent type of neuronal dysfunction, likely comprising both aging- and AD-related components.

In Vivo Functional Properties of Somatic Ca^{2+} Stores in Silent, Normal, and Hyperactive Cells. To test whether intracellular Ca^{2+} stores contribute to neuronal hyperactivity, we established an in vivo approach for probing their functional state. For this purpose, we locally pressure-applied an agonist of ryanodine receptors (RyRs), caffeine, to the cells of interest (Fig. 2*A*). To counteract the diffusion- and microcirculation-related drug dilution, in vivo drugs are usually applied at concentrations ~10-fold higher than the ones used in in vitro recordings (28, 29). For caffeine, however, this was not possible due to the solubility issue. Therefore, we increased reliability of caffeine-induced in vivo Ca^{2+} transients by boosting the Ca^{2+} content of the intracellular Ca^{2+} stores (30), and thus sensitizing RyRs to low concentrations of caffeine (31, 32). To do so, we first pressure-applied a glutamate receptor agonist NMDA followed by caffeine using a "double-pipette technique" (Fig. 2*A*). A red fluorescent dye, Alexa 594 (AF 594), was routinely added to all pressure-applied

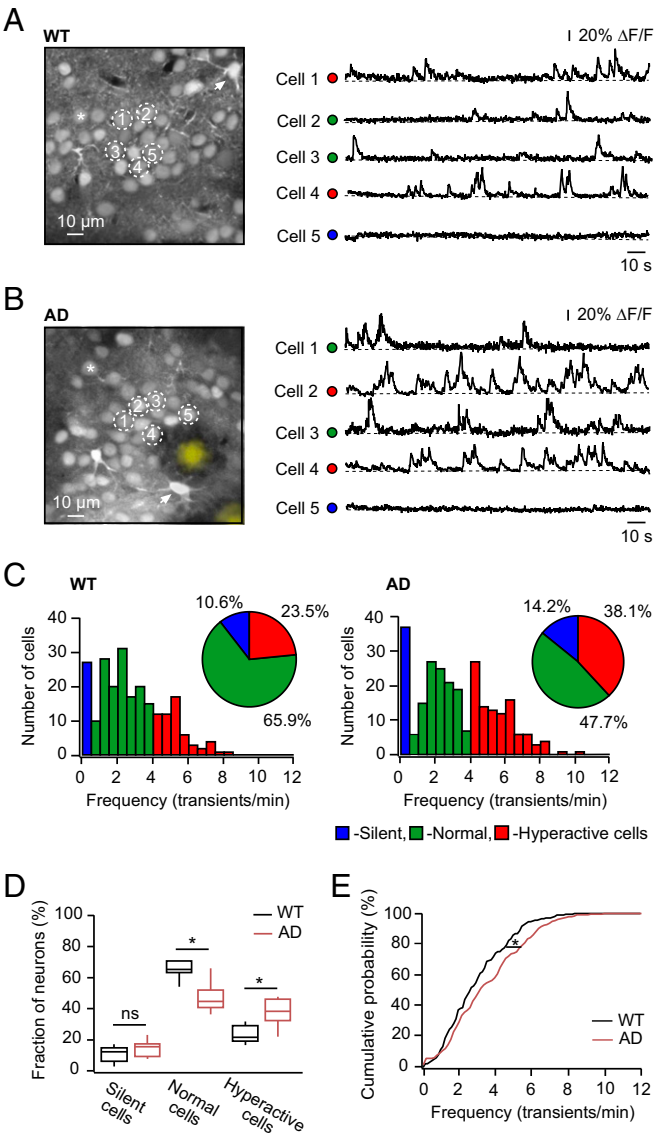

Fig. 1. Fraction of hyperactive neurons is high in 10- to 14-mo-old WT and AD mice. (*A* and *B*, *Left*) Maximum intensity projection images of layer 2/3 in the frontal/motor cortex of a WT mouse (*A*; 167- to 173-μm depth) and an AD mouse (*B*; 172- to 178-μm depth). Asterisks indicate one of many neurons within the field of view. Arrows point to astrocytes. Dark areas around the plaques in *B* are likely to be occupied by microglial cells, which are not labeled by OGB-1 AM (64). Plaques in *B* also bind OGB-1 AM (27). Here and below, plaques labeled by OGB-1 are colored yellow. Spontaneous Ca^{2+} transients (*A* and *B*, *Right*) were recorded simultaneously from neurons marked with respective numbers in the corresponding panel (*A* and *B*, *Left*). Here and below, the dots in front of the traces are color-coded according to the frequency of spontaneous Ca^{2+} transients: blue for silent cells, green for normal cells, and red for hyperactive cells. ΔF/F, relative change in fluorescence. (*C*) Histograms showing the frequency distribution of spontaneous Ca^{2+} transients in WT (*Left*; n = 226 cells in nine mice) and AD (*Right*; n = 260 cells in 10 mice) mice. (*Insets*) Pie charts showing the fractions of silent (blue) cells, normal (green) cells, and hyperactive (red) cells. The distributions are significantly different between the two mouse strains (χ^2 test: df = 2, $P < 0.01$). (*D*) Box-and-whisker plot illustrating median (per mouse) fractions of different cell types in WT (black, n = 9) and AD (crimson, n = 10) mice. The fraction of normal cells is significantly smaller and the fraction of hyperactive cells is significantly larger in AD compared with WT mice. The fraction of silent cells is similar in the two mouse strains [Student's t test: $t_{17} = 1.59$, $P = 0.39$ (silent cells); $t_{17} = 4.66$, $P < 0.01$ (normal cells); and $t_{17} = 4.26$, $P < 0.01$ (hyperactive cells)]. ns, not significant. (*E*) Cumulative probability function showing a significant shift toward a higher frequency of spontaneous Ca^{2+} transients in AD compared with WT mice (Kolmogorov–Smirnov test: $D = 0.15$, $P < 0.01$). *$P < 0.05$ in *D* and *E*.

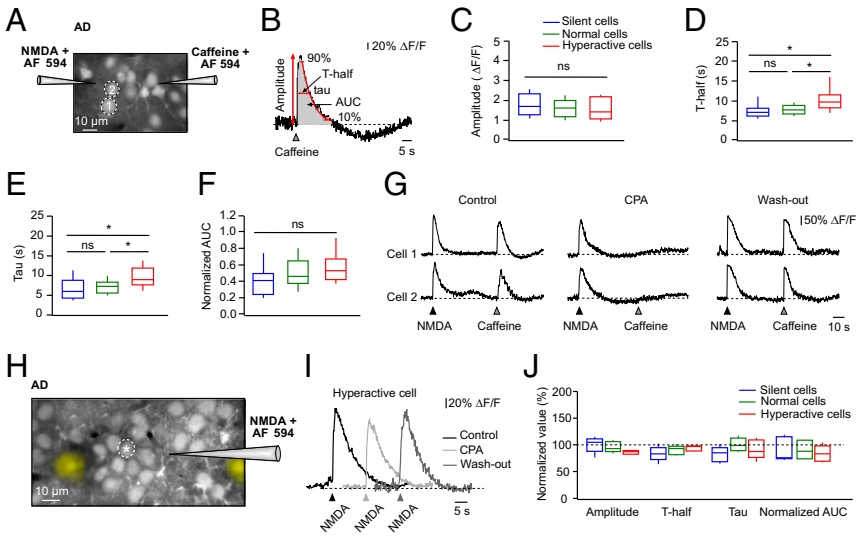

Fig. 2. In vivo properties of the somatic intracellular Ca^{2+} stores in silent, normal, and hyperactive cells from amyloid-depositing mice. (*A*) Maximum intensity projection image (155- to 161-µm depth) of layer 2/3 in the frontal/motor cortex of an AD mouse. Locations of 10 mM NMDA and 80 mM caffeine-containing pipettes are indicated. AF 594 (50 µM) was routinely added to all pipette solutions. (*B*) Caffeine-induced Ca^{2+} transient. Here and below, the triangle indicates the time point of application. The schematic illustrates parameters of Ca^{2+} transients analyzed in this study (amplitude, T-half, tau, and AUC). ΔF/F, relative change in fluorescence. Box-and-whisker plots illustrate amplitude (*C*), T-half (*D*), tau (*E*), and normalized AUC (*F*; $AUC_{Caffeine}/AUC_{AF\ 594}$) of caffeine-induced Ca^{2+} transients in silent (blue; $n = 13$ cells in five mice), normal (green; $n = 21$ cells in five mice), and hyperactive (red; $n = 17$ cells in five mice) cells in AD mice. Amplitude and normalized AUC are similar in the different cells types (one-way ANOVA: $F_{2,48} = 0.88$, $P = 0.42$ for amplitude and $F_{2,48} = 1.68$, $P = 0.20$ for normalized AUC). The T-half and tau of hyperactive cells are significantly higher [T-half; one-way ANOVA: $F_{2,48} = 6.24$, $P = 0.01$ (hyperactive vs. silent cells), $P = 0.01$ (hyperactive vs. normal cells), and $P = 0.99$ (silent vs. normal cells); tau: $F_{2,48} = 6.49$, $P < 0.01$ (hyperactive vs. silent cells), $P = 0.01$ (hyperactive vs. normal cells), and $P = 0.99$ (silent vs. normal cells)]. ns, not significant. (*G*) Evoked Ca^{2+} transients recorded from neurons labeled with respective numbers in *A* before, during, and after application of 400 µM CPA. (*H*) Maximum intensity projection image (169- to 175-µm depth) of layer 2/3 in the frontal/motor cortex of an AD mouse. The location of the pipette used for NMDA application (10 mM) is indicated. (*I*) NMDA-induced Ca^{2+} transients recorded from a hyperactive cell marked with an asterisk in *H* before (black), during (light gray), and after (dark gray) application of CPA. (*J*) Box-and-whisker plot illustrating the CPA effect on amplitude, T-half, tau, and normalized AUC of NMDA-induced transients in silent, normal, and hyperactive cells ($n = 5$ mice). All values obtained under CPA are normalized to respective control values. The dashed line is drawn at 100%. In the presence of CPA, there is no significant change in all parameters for all cell types [two-way repeated measures ANOVA: $F_{4,48} = 1.62$, $P = 0.18$]. *$P < 0.05$ in *D* and *E*.

drug-containing solutions to visualize the application pipettes and the approximate size of the drug-affected area.

Neuronal caffeine-induced Ca^{2+} transients in WT and AD mice were compared using the following parameters (Fig. 2*B*): amplitude, the width of the transient at half-maximal amplitude (T-half), decay time constant (tau), and area under the curve (AUC). The AUCs of AF 594 signals were used as a normalization factor to assess the relative amounts of agonists applied to neurons of WT and AD mice. The latter were similar under our experimental conditions (Fig. S1 *A* and *B*). Somatic caffeine-induced Ca^{2+} transients in layer 2/3 neurons of AD mice had similar amplitudes, but significantly larger T-half, tau, and normalized AUC ($AUC_{Caffeine}/AUC_{AF\ 594}$) compared with their counterparts recorded in neurons from WT mice (Fig. S1 *C–F*). No significant difference was detected for all four parameters (amplitude, T-half, tau, and normalized AUC) when comparing NMDA-induced Ca^{2+} transients in both mouse strains (Fig. S1 *G–J*). Next, we analyzed caffeine-induced Ca^{2+} transients separately in silent, normal, and hyperactive cells and found that transients in silent and normal cells in AD mice were similar to each other but significantly different in their T-half and tau from transients recorded in hyperactive cells (Fig. 2 *C–F*). In contrast, silent, normal, and hyperactive cells in WT mice were similar to each other for all four parameters analyzed [9 silent, 42 normal, and 12 hyperactive cells from five mice; one-way ANOVA: $F_{2,60} = 0.29$, $P = 0.75$ (amplitude); $F_{2,60} = 0.40$, $P = 0.67$ (T-half); $F_{2,60} = 2.19$, $P = 0.12$ (tau); and $F_{2,60} = 1.30$, $P = 0.28$ (normalized AUC)]. When comparing silent, normal, and hyperactive cells between the two mouse strains, the caffeine-induced Ca^{2+} transients in silent cells were similar, whereas normal and, especially, hyperactive cells in AD mice showed significantly longer caffeine-induced Ca^{2+} transients (Fig. S2 *A–D*). Of note, NMDA-induced Ca^{2+} transients in silent, normal, and hyperactive cells did not differ between WT and AD mice (Fig. S2 *E–H*).

Next, we estimated the in vivo concentration of cyclopiazonic acid (CPA), a known reversible inhibitor of the endoplasmic reticulum (ER) Ca^{2+} pumps, blocking caffeine-induced Ca^{2+} signals (30). A topical application of 400 µM CPA for 30 min completely and reversibly inhibited caffeine-induced Ca^{2+} signals (Fig. 2*G*), thus enabling us to test the in vivo contribution of intracellular Ca^{2+} stores to endogenous as well as agonist-evoked Ca^{2+} transients. To test whether Ca^{2+}-induced Ca^{2+} release (CICR) from intracellular Ca^{2+} stores contributes to NMDA-induced Ca^{2+} transients in AD mice, we compared the four aforementioned parameters in the presence and the absence of CPA (Fig. 2 *H–J*). In contrast to what could be expected based on in vitro data (33), in vivo CPA treatment had no effect on the NMDA-induced Ca^{2+} transients (Fig. 2*J*).

Taken together, these data suggest that an overfilling of somatic intracellular Ca^{2+} stores in AD mice in vivo is much less prominent than in vitro and is largely restricted to hyperactive cells.

The Role of Intracellular Ca^{2+} Stores for AD-Related Neuronal Hyperactivity. To test whether intracellular Ca^{2+} stores contribute to AD-related neuronal hyperactivity, we measured endogenous network activity in the absence and presence of CPA. In WT mice, the fractions of silent, normal, and hyperactive cells remained stable before, during, and after the CPA treatment (Fig. 3 *B* and *E* and Fig. S3 *A* and *C*), as did the frequency, amplitude, T-half, and tau of spontaneous Ca^{2+} transients in

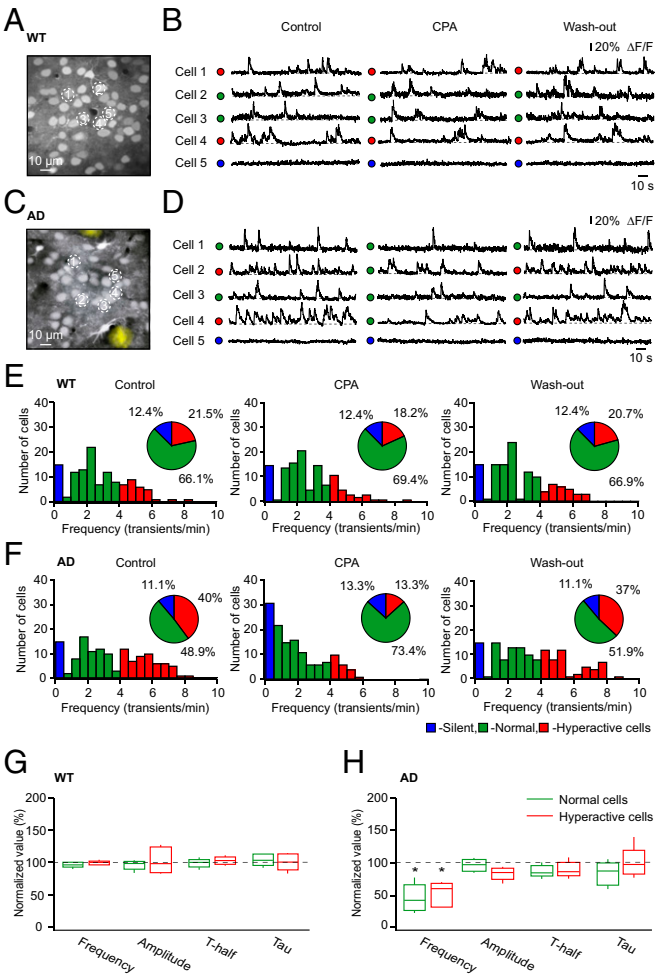

Fig. 3. Emptying the intracellular Ca^{2+} stores selectively reduces neuronal hyperactivity in amyloid-depositing mice. Maximum intensity projection images of layer 2/3 in the frontal/motor cortex of a WT mouse (*A*; 157- to 162-μm depth) and an AD mouse (*C*; 161- to 166-μm depth) are shown. (*B* and *D*) Spontaneous Ca^{2+} transients recorded before, during, and after topical application of CPA from neurons labeled with respective numbers in *A* and *C*. Note that CPA strongly reduces the fraction of hyperactive cells in AD mice only. ΔF/F, relative change in fluorescence. (*E* and *F*) Histograms showing the frequency distributions of spontaneous Ca^{2+} transients recorded before, during, and after topical application of CPA in WT ($n = 121$ cells in five mice) and AD ($n = 135$ cells in five mice) mice. (*Insets*) Pie charts showing the fractions of silent (blue), normal (green), and hyperactive (red) cells under the respective conditions. Box-and-whisker plots show the effect of CPA on the median (per mouse) frequency, amplitude, T-half, and tau of spontaneous Ca^{2+} transients recorded from normal and hyperactive neurons in five WT mice (*G*) and five AD mice (*H*). Note that CPA significantly decreased the frequency of spontaneous Ca^{2+} transients in both normal and hyperactive cells in AD mice [two-way repeated measures ANOVA: $F_{4,32} = 17.17$, $P < 0.01$ for both normal and hyperactive cells] without affecting Ca^{2+} transients in WT mice (two-way repeated measures ANOVA; $F_{4,32} = 0.43$, $P = 0.78$). $^*P < 0.05$ in *H*.

individual cells (Fig. 3*G*). In contrast, CPA treatment caused a significant reduction of neuronal hyperactivity in AD mice (frequency under CPA compared with control: 57.5 ± 32.25%; Student's *t* test: $t_4 = 6.56$, $P < 0.01$), leading to efficient suppression of this AD-related pathology in the entire neuronal population (Fig. 3 *D* and *F* and Fig. S3 *B* and *D*). At the single-cell level, CPA treatment significantly lowered the frequency of spontaneous Ca^{2+} transients in normal and hyperactive cells (Fig. 3*H*). Similar results were obtained using a topical application of the RyR blocker dantrolene (100 μM for 30 min), but dantrolene influenced hyperactive cells only and did not differentiate between AD and WT mice (Fig. S4 *A* and *B*).

Taken together, these results identify the intracellular Ca^{2+} stores as a key element controlling neuronal hyperactivity in vivo. Whereas emptying the intracellular Ca^{2+} stores selectively reduces AD-related hyperactivity, both aging- and AD-related components were efficiently suppressed by blocking RyRs.

AD-Related Mutation in PS1 Is a Significant Factor Controlling Store-Mediated Neuronal Hyperactivity. In general, neuronal hyperactivity can be caused by the presence of amyloid species (9, 15), a proinflammatory environment in the vicinity of amyloid plaques (34), or modified properties of excitatory synaptic transmission caused by AD-related presenilin mutation (3). To assess the mechanisms underlying store-mediated neuronal hyperactivity in $APP_{swe}/PS1_{G384A}$ mice, we switched to PS45 mice, which contain the same presenilin mutation as $APP_{swe}/PS1_{G384A}$ mice but lack both amyloid deposition and plaque-related neuroinflammation (Fig. S5). Surprisingly, neuronal networks in both homo- and heterozygous 10- to 14-mo-old PS45 mice contained large fractions of hyperactive cells (Fig. 4 *E* and *F*), similar to neuronal networks in AD mice [χ^2 test: df = 2, $P = 0.36$ (AD vs. homozygous PS45 mice) and $P = 0.11$ (AD vs. heterozygous PS45 mice)]. Compared with age-matched WT mice, the frequency distribution of Ca^{2+} transients in homo- and heterozygous PS45 mice was significantly shifted to higher values (Fig. S6*B*). There was no significant difference in the fraction of silent, normal, and hyperactive cells; the overall frequency distribution; or the amplitude, T-half, and tau of Ca^{2+} transients in individual cells between homo- and heterozygous PS45 mice, suggesting that a single copy of the mutated gene is sufficient to produce a full-blown effect (Fig. S6 *A*–*E*).

In both homo- and heterozygous PS45 mice, CPA treatment significantly reduced the frequency of Ca^{2+} transients in individual neurons [frequency under CPA compared with control: 50 ± 8.5% in $PS45^{tg/tg}$ (transgenic) and 67 ± 23.5% in $PS45^{tg/+}$ mice; Student's *t* test: $t_4 = 23.12$, $P < 0.01$ for $PS45^{tg/tg}$ and $t_4 = 6.10$, $P < 0.01$ for $PS45^{tg/+}$] and in the fraction of hyperactive cells, mimicking in this respect data obtained in AD mice (Fig. 4 *E*–*H* and Fig. S6 *F* and *G*). Consistently, dantrolene treatment also significantly reduced the frequency of Ca^{2+} transients in hyperactive cells (Fig. S4*C*). Interestingly, store-mediated neuronal hyperactivity was also observed in 6- to 7-mo-old PS45 mice (Fig. 5), at the age at which no hyperactivity is seen in WT mice (14) (Fig. 5*D*). Similar to data obtained in 10- to 14-mo-old PS45 and AD mice, treatment of 6- to 7-mo-old PS45 mice with CPA significantly reduced the frequency of Ca^{2+} transients in individual neurons (frequency under CPA compared with control: 58 ± 10.5%; Student's *t* test: $t_4 = 17.16$, $P < 0.01$) and the fraction of hyperactive cells (Fig. 5 *C*, *E*, and *F*).

To test whether store-mediated neuronal hyperactivity can be observed in the absence of the presenilin mutation, we conducted experiments similar to those described above (Fig. 4) in age-matched APP_{swe} mice (Fig. S7). At this age, the fraction of hyperactive cells in APP_{swe} mice was not significantly different from that in WT mice (Student's *t* test: $t_{12} = 1.48$, $P = 0.49$), confirming earlier findings that AD-related symptoms in these mice develop later (16, 35). Surprisingly, we observed a significantly larger fraction of normal cells and a significantly smaller fraction of silent cells in APP_{swe} mice compared with WT mice [Student's *t* test: $t_{12} = 3.55$, $P = 0.01$ (silent cells) and $t_{12} = 3.98$, $P < 0.01$ (normal cells)]. Nonetheless, the fraction of hyperactive cells in APP_{swe} mice was significantly higher than that in young PS45 mice (Student's *t* test: $t_8 = 3.32$, $P = 0.03$). However, in contrast to our findings in both young and age-matched PS45 mice, emptying the

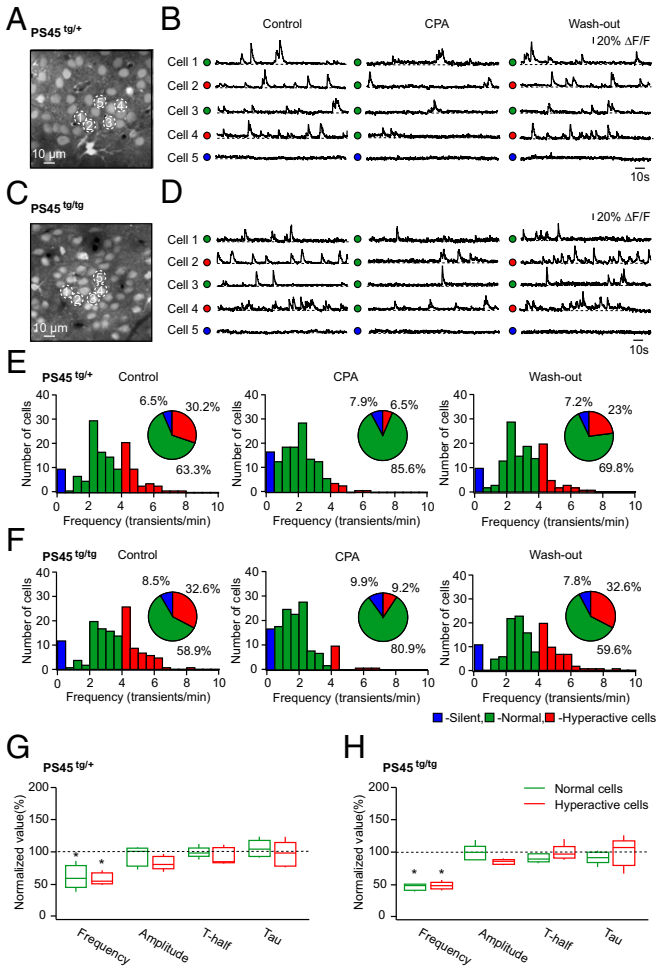

Fig. 4. Store-mediated neuronal hyperactivity in PS1 mouse mutants. Maximum intensity projection images of layer 2/3 in the frontal/motor cortex of a PS45$^{tg/+}$ mouse (*A*; 158- to 164-μm depth) and a PS45$^{tg/tg}$ mouse (*C*; 161- to 167-μm depth) are shown. (*B* and *D*) Spontaneous Ca^{2+} transients recorded from neurons marked with respective numbers in *A* and *C* before, during, and after topical application of CPA. ΔF/F, relative change in fluorescence. Histograms show the frequency distributions of spontaneous Ca^{2+} transients in PS45$^{tg/+}$ (*E*; n = 139 cells in five mice) and PS45$^{tg/tg}$ (*F*; n = 141 cells in five mice). (*Insets*) Pie charts showing the fractions of silent (blue), normal (green), and hyperactive (red) cells recorded before, during, and after topical application of CPA. Under control conditions, there is no significant difference in the fractions of silent, normal, and hyperactive cells between the two PS45 strains (χ^2 test: df = 2, P = 0.73), but note a remarkable decrease in the fraction of hyperactive cells in both mouse strains in the presence of CPA. Box-and-whisker plots show the effect of CPA on the median (per mouse) frequency, amplitude, T-half, and tau of spontaneous Ca^{2+} transients recorded in normal and hyperactive cells in five PS45$^{tg/+}$ (*G*) and five PS45$^{tg/tg}$ (*H*) mice. Note that CPA significantly decreased the frequencies of Ca^{2+} transients recorded in both normal and hyperactive cells [two-way repeated measures ANOVA: $F_{4,32}$ = 31.07, P < 0.01 for both comparisons in PS45$^{tg/+}$ and $F_{4,32}$ = 50.31, P < 0.01 for both comparisons in PS45$^{tg/tg}$]. *P < 0.05 in *G* and *H*.

intracellular Ca^{2+} stores in APP_{swe} mice had no effect on neuronal hyperactivity (Fig. S7 *B–D*).

In summary, these in vivo data identify the G384A mutation in PS1 as a significant factor mediating neuronal hyperactivity in PS45 and AD mice. The PS1-mediated hyperactivity is detected as early as 6 mo of age (~10% of all cells are hyperactive). The fraction of hyperactive cells increases significantly as the time passes, reaching ~30% of the entire neuronal population in 10- to 14-mo-old animals.

Hyperactive Cells Are Likely Driven by Synapses with Higher Release Probability. To test whether normal and hyperactive cells in PS45 mice are activated by the surrounding network in a similar way, we monitored spontaneous Ca^{2+} transients in these cells before and every 10 min during topical application of the activity-dependent NMDA receptor blocker MK-801 (Fig. 6). In the presence of MK-801, the frequency of spontaneous Ca^{2+} transients in both normal and hyperactive cells gradually decreased and finally reached a plateau level (Fig. 6 *A–C*). The amplitudes of somatic Ca^{2+} transients measured in both cell

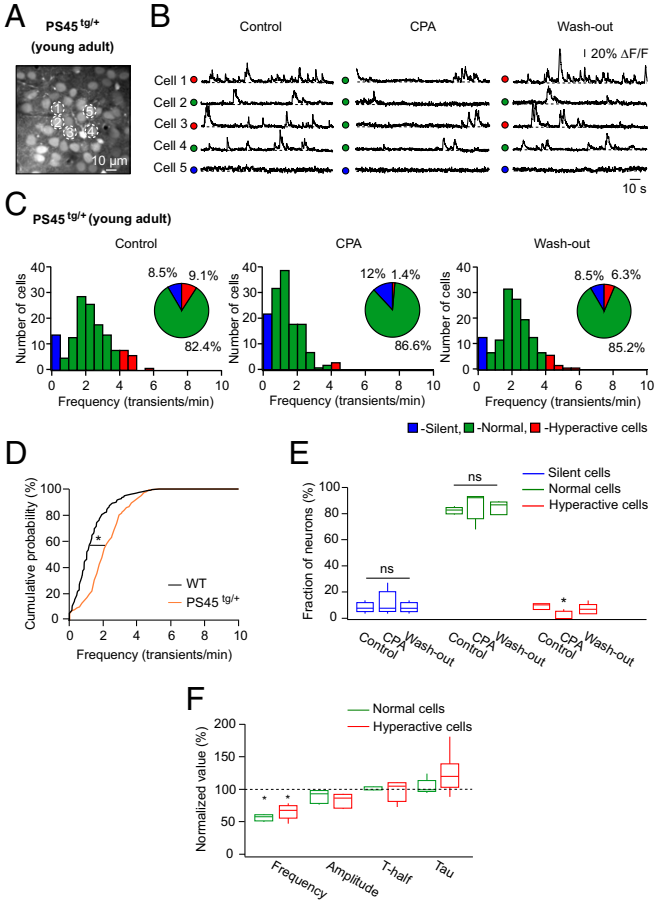

Fig. 5. CPA selectively reduces the fraction of hyperactive cells in young adult PS45 mice. (*A*) Maximum intensity projection image (163- to 169-μm depth) of layer 2/3 in the frontal/motor cortex of a 6-mo-old PS45$^{tg/+}$ mouse. (*B*) Spontaneous Ca^{2+} transients recorded from neurons marked with respective numbers in *A* before, during, and after topical application of CPA. ΔF/F, relative change in fluorescence. (*C*) Histograms showing the frequency distributions of spontaneous Ca^{2+} transients recorded before, during, and after topical application of CPA in 6- to 7-mo-old PS45$^{tg/+}$ mice (n = 142 cells in five mice). (*Insets*) Pie charts showing fractions of silent (blue), normal (green), and hyperactive (red) cells under the aforementioned conditions. (*D*) Cumulative probability functions showing a significant shift of frequency distribution in PS45$^{tg/+}$ (orange; n = 142 cells in five mice) compared with WT (black; n = 233 cells in eight mice) mice (Kolmogorov–Smirnov test; D = 0.44, P < 0.01). (*E*) Box-and-whisker plot illustrating median (per mouse) fractions of the three cell types in five mice. Note a small but significant decrease in the fraction of hyperactive cells under CPA (Friedman's test: Q = 8.32, P = 0.02). ns, not significant. (*F*) Box-and-whisker plot illustrating the effect of CPA on the median frequency, amplitude, T-half, and tau of spontaneous Ca^{2+} transients recorded in normal (green) and hyperactive (red) cells. Note that CPA significantly decreased the frequency of both normal and hyperactive cells [two-way repeated measures ANOVA: $F_{4,32}$ = 28.90, P < 0.01 for both comparisons]. *P < 0.05 in *D–F*.

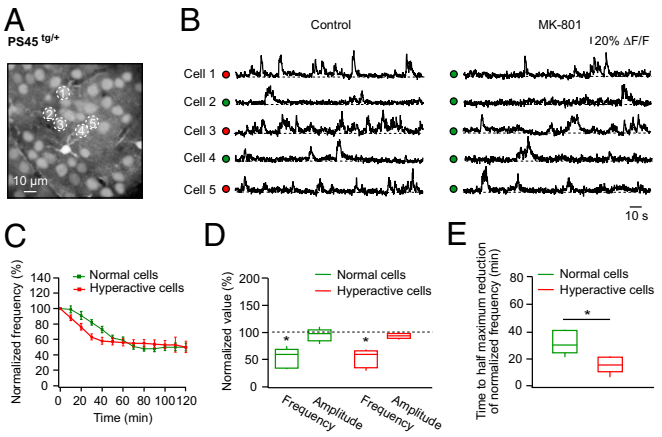

Fig. 6. Activity-dependent blockade of postsynaptic NMDA receptors reveals higher release probability of synapses driving spontaneous activity in hyperactive cells. (*A*) Maximum intensity projection image of layer 2/3 in the frontal/motor cortex of a PS45$^{tg/+}$ mouse (177- to 183-µm depth). (*B*) Spontaneous Ca^{2+} transients recorded from neurons labeled with respective numbers in *A* under control conditions (*Left*) and after 50 min of topical application of 200 µM MK-801 (*Right*). ΔF/F, relative change in fluorescence. (*C*) Normalized frequency of spontaneous Ca^{2+} transients plotted against the duration of the topical MK-801 application measured in normal (green; $n = 34$ cells in five mice) and hyperactive (red; $n = 20$ cells in five mice) cells. Data shown in this graph represent mean values ± SEM. (*D*) Box-and-whisker plot illustrating the maximal effect of MK-801 on the frequency and amplitude of spontaneous Ca^{2+} transients in normal (green) and hyperactive (red) cells. All values measured under MK-801 are normalized to respective control values. Note a significant reduction of frequency in both normal and hyperactive cells [two-way repeated measures ANOVA: $F_{2,16} = 48.37$, $P < 0.01$ for both comparisons], whereas amplitudes are not affected [$P = 0.99$ (normal cells) and $P = 0.86$ (hyperactive cells)]. (*E*) Box-and-whisker plot illustrating the time needed for normal (green) and hyperactive (red) cells to reach the half-maximal reduction of the frequency of spontaneous Ca^{2+} transients. This time period is significantly shorter for hyperactive cells compared with normal cells (Student's *t* test: $t_8 = 3.48$, $P < 0.01$). *$P < 0.05$ in *D* and *E*.

types after reaching the plateau were unaffected by MK-801 treatment (Fig. 6*D*), suggesting that these were mainly caused by somatic action potential firing with a minor contribution of NMDA receptor-mediated Ca^{2+} influx. Interestingly, the time required to reach a half-maximal reduction of frequency was significantly shorter for hyperactive cells compared with that measured for normal cells (Fig. 6*E*).

These data suggest that somatic Ca^{2+} transients of layer 2/3 neurons in PS45 mice depend on activation of postsynaptic NMDA receptors and that postsynaptic NMDA receptors in hyperactive cells have a higher open probability (36) compared with NMDA receptors in normal cells. In view of the similar intrinsic excitability of normal and hyperactive cells in these mice (14), the latter may be due to an increased presynaptic release probability of the respective glutamatergic synapses.

The Role of Presynaptic Intracellular Ca^{2+} Stores. Because presynaptic release probability is directly linked to Ca^{2+} availability within the axonal terminal (24, 37), we tested the contribution of presynaptic Ca^{2+} stores to the ongoing spontaneous activity in PS45 mice. To do so, we studied two different inputs to layer 2/3. First, we labeled neurons in layers 5 and 6 of the motor cortex with adenoassociated virus (AAV)-GCaMP6f and analyzed in vivo spontaneous Ca^{2+} transients in the axonal boutons of these cells projecting to the dendrites of layer 2/3 neurons (38) (Fig. 7 *A–E*). The transients were monitored before, during, and after topical application of CPA (Fig. 7*D*), and their frequencies and amplitudes were analyzed across the three conditions. Application of CPA for 30 min significantly and reversibly decreased both the frequency and amplitude of presynaptic Ca^{2+} transients (Fig. 7*E*). Second, we monitored long-range axonal projections originating in the barrel cortex (39) and obtained similar results (Fig. 7*F*). To test whether the observed effect of CPA on axonal boutons is caused by inhibition of layer 2/3 cells in the motor cortex and subsequent modulation of the reciprocal connections between the motor and the barrel cortex, we repeated the above experiments in the presence of high concentrations of glutamate receptor blockers. Topical application of 6-cyano-7-nitroquinoxaline-2,3-dione (100 µM) and 2-amino-5-phosphonopentanoic acid (200 µM) to the motor cortex completely blocked spontaneous Ca^{2+} transients in layer 2/3 neurons (Fig. S8 *A–C*), without affecting the activity of presynaptic boutons of axons originating in the barrel cortex (Fig. S8*D*). Also, under these conditions, CPA significantly reduced the frequency, as well as the amplitude, of axonal Ca^{2+} transients (Fig. 7*G*). Thus, the observed effects of CPA are caused by blockade of intracellular Ca^{2+} stores in axonal boutons, because (*i*) the cell bodies of the neurons in the barrel cortex were located far from the craniotomy, and thus were unlikely to be influenced by CPA, and (*ii*) the effects persisted during blockade of the local network activity in the motor cortex.

Further, we tested whether intracellular Ca^{2+} stores control the pattern of spontaneous Ca^{2+} transients in axonal boutons. To this end, we classified axonal Ca^{2+} transients as either single transients or bursts according to criteria described in *Materials and Methods* (Fig. 7 *H* and *J*). Despite a significant reduction in the frequency of both single transients and bursts upon CPA treatment (one-way ANOVA: $F_{2,12} = 10.57$, $P < 0.01$ for both comparisons), the overall patterns of Ca^{2+} transients (i.e., the fractions of single transients and bursts) remained stable (Fig. 7 *I* and *K*).

In WT mice (Fig. S9), the axonal projections from the barrel to motor cortex showed similar amplitudes of spontaneous Ca^{2+} transients compared with PS45 mice ($n = 80$ boutons in five WT mice and $n = 84$ boutons in five PS45 mice; Kolmogorov–Smirnov test: $D = 0.86$, $P = 0.86$), but a different activity pattern with a significantly higher fraction of single transients (Fig. S9*E*) and, respectively, a smaller fraction of bursts. In contrast to the data obtained in PS45 mice, CPA treatment in WT mice changed neither the frequency nor the amplitude of presynaptic Ca^{2+} transients (Fig. S9 *C* and *D*). The overall activity pattern of Ca^{2+} transients (i.e., the fractions of single transients and bursts) also remained stable in the presence of CPA (Fig. S9*B*).

Thus, compared with WT mice, PS45 mice have a different presynaptic activity pattern with a higher fraction of bursts and a significant contribution of axonal intracellular Ca^{2+} stores, which control both the amplitude and the frequency of presynaptic Ca^{2+} transients, thereby controlling the presynaptic neurotransmitter release.

The Role of Dendritic Intracellular Ca^{2+} Stores in Postsynaptic Cells. To test how mutant PS1-mediated dysfunction of Ca^{2+} stores impacts dendritic Ca^{2+} transients in postsynaptic cells, we examined the effect of CPA on spontaneous Ca^{2+} transients in dendritic branches of layer 2/3 pyramidal neurons, which were loaded with OGB-1 by means of single-cell electroporation (Fig. 8*A*; further details are provided in *Materials and Methods*). We first classified the cells as normal or hyperactive by recording the spontaneous somatic Ca^{2+} transients, and thereafter switched to recording of spontaneous Ca^{2+} transients in apical dendritic branches. The transients were monitored before, during, and after topical application of CPA (Fig. 8*B*), similar to the protocol used for somatic recordings (Fig. 3). Depletion of intracellular Ca^{2+} stores by CPA decreased the frequency of spontaneous dendritic Ca^{2+} transients in normal and hyperactive cells to a similar extent (Fig. 8*C*). We did not observe any difference between the effects of CPA on somatic (Fig. 4*G*) and dendritic

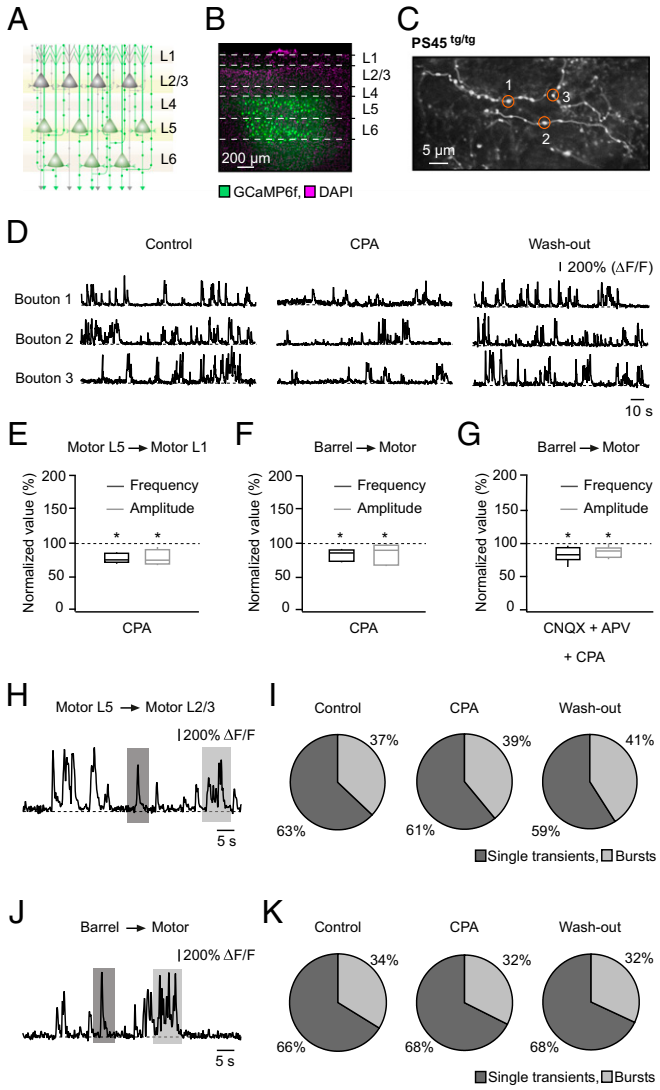

Fig. 7. Contribution of presynaptic Ca^{2+} stores to ongoing spontaneous activity in PS45 mice. (*A*) Scheme of the experimental arrangement. Layer 5/6 neurons of the motor cortex (colored in green) were virally labeled with GCaMP6f, and axonal projections of these cells into layer 1, close to dendrites of unlabeled layer 2/3 neurons (colored in gray), were analyzed. Thin lines are axonal projections, and filled circles are axonal boutons. (*B*) Image of a fixed brain slice illustrating the intracortical distribution of GCaMP6f staining (green). The slice was counterstained with DAPI (magenta). Dashed lines indicate boundaries between cortical layers. (*C*) Maximum intensity projection in vivo image (21- to 25-µm depth) of GCaMP6f-positive axons in layer 1 of the motor cortex in a $PS45^{tg/tg}$ mouse. (*D*) Spontaneous Ca^{2+} transients recorded from axonal boutons labeled with respective numbers in *C* before, during, and after topical application of CPA. ΔF/F, relative change in fluorescence. Box-and-whisker plots illustrate the CPA effects on the median (per mouse) frequency and amplitude of spontaneous Ca^{2+} transients in boutons of ascending (*E*; $n = 92$ boutons in five mice) and long-range (*F*; $n = 84$ boutons in five mice) projections. Frequency and amplitude were significantly reduced under CPA [ascending projections: one-way repeated measures ANOVA: $F_{1.68,6.73} = 14.03$, $P < 0.01$ (frequency) and $P < 0.05$ (amplitude); long-range projections: one-way repeated measures ANOVA: $F_{1.24,4.95} = 14.97$, $P = 0.01$ (frequency) and $P < 0.05$ (amplitude)]. (*G*) Box-and-whisker plot illustrating CPA effects on the median (per mouse) frequency and amplitude of spontaneous Ca^{2+} transients under 6-cyano-7-nitroquinoxaline-2,3-dion (CNQX) and 2-amino-5-phosphonopentanoic acid (APV) in axonal boutons of long-range projections ($n = 53$ boutons in seven mice). Frequency and amplitude were significantly reduced under CPA [one-way repeated measures ANOVA; $F_{1.68,10.1} = 10.24$, $P < 0.01$(frequency) and $P = 0.02$ (amplitude)]. Spontaneous Ca^{2+} transients recorded from axonal boutons of ascending (*H*) and long-range (*J*) projections are shown. Dark-gray boxes mark single transients, and light-gray boxes mark bursts. Pie charts show the fractions of single transients (dark gray) and bursts (light gray) in ascending (*I*) and long-range (*K*) projections before, during, and after topical application of CPA (from same dataset as in *E* and *F*). *$P <$ 0.05 in *E*–*G*.

(Fig. 8*C*) Ca^{2+} transients in either normal or hyperactive cells (two-way ANOVA: $F_{1,24} = 0.01$, $P = 0.97$ for somatic vs. dendritic cells and $F_{1,24} = 0.02$, $P = 0.90$ for normal vs. hyperactive cells). In WT mice, CPA affected neither the frequency nor amplitude of spontaneous dendritic Ca^{2+} transients (Fig. S10 *A*–*C*), in agreement with the lack of CPA effect in somatic recordings (Fig. 3 *B*, *E*, and *G*).

Next, we analyzed spontaneous dendritic Ca^{2+} transients obtained in paired branch recordings. The transients occurring only in one of the two branches were considered local, whereas those occurring simultaneously in both branches were considered synchronous (Fig. 8*D*). Although there was no difference in the amplitude of either local or synchronous dendritic Ca^{2+} transients recorded in WT and PS45 mice under control conditions (Mann–Whitney test, $P \geq 0.05$ for all comparisons; $n = 5$–6 mice for each group), the CPA treatment significantly reduced the amplitudes of dendritic Ca^{2+} transients in hyperactive cells of PS45 mice only (Fig. 8*E* and Fig. S10*C*). To analyze the effect of CPA in more detail, we compared the fractions of local and synchronous dendritic Ca^{2+} transients in the presence and absence of CPA (Fig. 8 *F* and *G*). In the presence of CPA, we observed a significant increase in the fraction of local dendritic Ca^{2+} transients and a proportional decrease in the fraction of synchronous Ca^{2+} transients in hyperactive cells (Fig. 8*G*). The values obtained in normal cells exhibited similar trends, but did not reach the level of significance. Interestingly, similar results were obtained for local dendritic Ca^{2+} transients of WT mice (Fig. S10 *D* and *E*).

In summary, our results show that intracellular Ca^{2+} stores control the frequency of somatic and dendritic Ca^{2+} transients in both normal and hyperactive cells in PS45 mice, but impact the amplitude of dendritic Ca^{2+} transients in hyperactive cells only. In addition, they suggest that intracellular Ca^{2+} stores are important for proper compartmentalization of dendritic Ca^{2+} signals in both WT and in PS45 mice. The latter is instrumental for correct information processing within the dendrites (40, 41).

Discussion

This study analyzes the in vivo function of intracellular Ca^{2+} stores and discovers their key role for AD-related neuronal hyperactivity. We show that hyperactivity of cortical neurons is part of healthy aging, but is significantly enhanced by AD-related mutations in presenilins. Importantly, an FAD-related mutation in only one allele of the PS1 gene (in the absence of any amyloid deposits or inflammation) is sufficient to bring hyperactivity within the cortical neural network to the level comparable to that found in AD mice. Our data further show that the PS1-mediated neuronal hyperactivity develops well before the aging-related hyperactivity as well as APP_{swe}-mediated hyperactivity and is mainly caused by a dysfunction of the intracellular Ca^{2+} stores in presynaptic boutons. Emptying the axonal Ca^{2+} stores significantly reduces both the amplitude and frequency of presynaptic Ca^{2+} transients in PS45 mice and, most importantly, normalizes neuronal network activity in both $APP_{swe}/PS1_{G384A}$ and PS45 mouse strains. Finally, our data suggest that dendritic Ca^{2+} stores contribute to synchronization of Ca^{2+} transients in neighboring dendritic branches.

Our results enable direct in vivo visualization of neuronal hyperactivity in the frontal/motor cortex of aging WT mice and

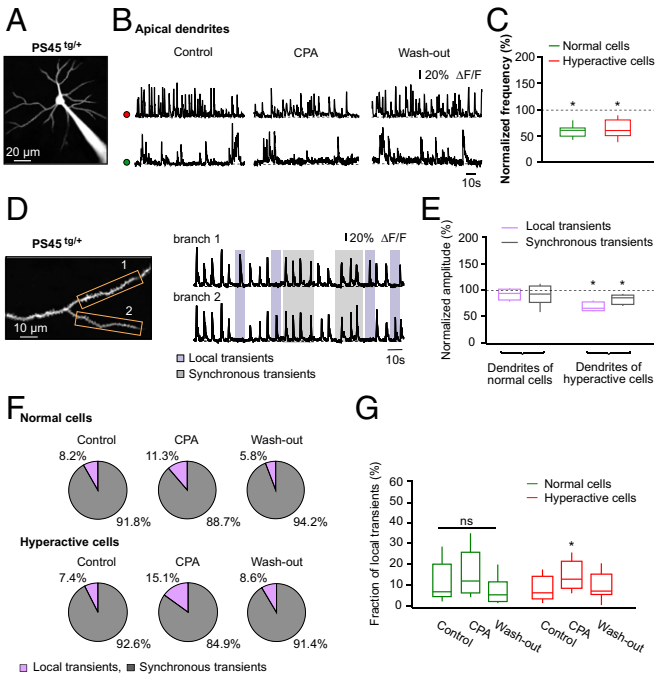

Fig. 8. Role of intracellular stores for dendritic Ca^{2+} signaling in postsynaptic cells of PS45 mice. (*A*) Maximum intensity projection image (160- to 180-µm depth) of an OGB-1–labeled layer 2/3 neuron in the frontal/motor cortex of a $PS45^{tg/+}$ mouse. (*B*) Spontaneous dendritic Ca^{2+} transients before, during, and after CPA application. Colored dots indicate the type of neuron (green, normal; red, hyperactive). ΔF/F, relative change in fluorescence. (*C*) Box-and-whisker plot showing the CPA effect on the median (per mouse) frequency of dendritic Ca^{2+} signals in normal (green; 40 dendrites, 14 cells in nine mice) and hyperactive (red; 34 dendrites, 14 cells in nine mice) cells. The frequency was significantly reduced in both cell types (one-way ANOVA: $F_{2,24} = 32.29$, $P < 0.01$ for both comparisons). (*D*) Maximum intensity projection image (153- to 157-µm depth) of apical dendritic branches of an OGB-1–labeled neuron (*Left*) and corresponding Ca^{2+} signals (*Right*) in two branches marked with respective numbers (*Left*). Purple boxes mark local transients, and gray boxes mark synchronous transients. (*E*) Box-and-whisker plot illustrating the CPA effect on the median (per mouse) amplitude of local (purple) and synchronous (gray) Ca^{2+} transients in dendrites of normal (30 dendrites, 10 cells in six mice) and hyperactive (26 dendrites, nine cells in six mice) cells. CPA selectively decreases amplitudes of local and synchronous Ca^{2+} transients in hyperactive cells [two-way ANOVA: $F_{2,30} = 10.52$, $P < 0.01$ (local transients) and $P = 0.02$ (synchronous transients)], without affecting those of normal cells [$P = 0.82$ (local transients) and $P = 0.47$ (synchronous transients)]. (*F*) Pie charts illustrating the fractions of local and synchronous dendritic transients recorded in normal (*Upper*; 30 dendritic branches in 10 cells) and hyperactive (*Lower*; 26 dendritic branches in nine cells) cells before, during, and after application of CPA. (*G*) Box-and-whisker plot showing median (per cell) fractions of local Ca^{2+} transients before, during, and after application of CPA in dendrites of normal (green; $n = 10$ cells in six mice) and hyperactive (red; $n = 9$ cells in six mice) cells. Categorical data in *F* show a trend toward an increase of local transients under store blockade, which is more pronounced in hyperactive cells. This trend reaches significance when analyzing median values per cell (as shown in *G*) using two-way repeated measures ANOVA ($F_{2,34} = 4.72$, $P = 0.04$). *$P < 0.05$ in *C*, *E*, and *G*.

show that cortical hyperactivity develops rather early, even before the animals are considered aged (42). These data substantiate previous less direct evidence obtained with different in vitro techniques in aged (24- to 32-mo-old) rats (43, 44). Whereas in vivo imaging revealed a high fraction of hyperactive cells in every animal tested (Fig. 1*D*), counting c-Fos^{+} neurons in aged rats treated with a subconvulsive dose of pilocarpine reported neuronal hyperactivity in animals with an impaired memory performance only (43). Interestingly, subclinical epileptiform activity, reflecting the hyperactivity of the underlying neural networks, was also observed in 10.5% of healthy 65-y-old humans (11), supporting the strong association between aging and cortical hyperactivity across mammalian species.

Compared with healthy aged subjects, the incidence of subclinical epileptiform activity increased significantly in patients with AD without a history of seizures. It was, for example, found in 42% of patients within the relatively young (55- to 68-y-old) AD cohort with a mild stage of disease (11). Similarly, compared with aging WT mice, the hyperactivity of cortical neurons increased significantly in age-matched AD mice and, even more surprisingly, in PS45 mice presenting with neither amyloidosis nor inflammation. PS45 mice were previously considered asymptomatic (45). Our results show, however, that in terms of neuronal hyperactivity as well as the Ca^{2+} store-dependent mechanism of its generation, PS45 mice highly resemble APP_{swe}/$PS1_{G384A}$ mice.

Based on our data, we hypothesize that neuronal hyperactivity in APP_{swe}/$PS1_{G384A}$ and PS45 mice is caused by malfunctional intracellular Ca^{2+} stores in presynaptic boutons mediating heightened neurotransmitter release and, as a consequence, neuronal hyperactivity. Emptying the Ca^{2+} stores decreases both the amplitude and frequency of presynaptic Ca^{2+} transients as well as neurotransmitter release at glutamatergic synapses and normalizes the strength of neuronal activity. In this respect, our data are entirely consistent with recent data of de Juan-Sanz et al. (24) showing that in primary dissociated hippocampal neurons, the filling state of axonal Ca^{2+} stores controls release probability at glutamatergic synapses. This process critically depends on the activity of ER Ca^{2+} pumps, as in our case, and, interestingly, on the recruitment of the ER Ca^{2+} sensor stromal interaction molecule 1 (STIM1) to presynaptic terminals, where it inhibits the action potential-evoked presynaptic Ca^{2+} influx. However, based on their in vitro data, the authors assume that the described mechanism represents a basic principle of the ER-mediated control of neurotransmitter release (24), whereas our in vivo data suggest that this mechanism is only functional in the presence of an AD-related mutation in PS1 and does not operate in WT mice, even under conditions of aging-related neuronal hyperactivity.

Further support for our hypothesis comes from the fact that the presynaptically active antiepileptic drug levetiracetam is able to reduce neuronal hyperactivity as well as behavioral abnormalities and to improve learning and memory in a mouse model of AD (46). Moreover, levetiracetam reduces hippocampal hyperactivity in patients with aMCI, increasing their task-related memory performance at the same time (12). Noteworthy, levetiracetam binds to the synaptic vesicle protein 2A (47), which is known to influence expression and trafficking of the presynaptic Ca^{2+} sensor synaptotagmin and to modulate Ca^{2+}-dependent neurotransmitter release (7). In addition, levetiracetam was shown to inhibit both RyR- and inositol trisphosphate receptor-mediated Ca^{2+} release in cell cultures (7).

While emphasizing an important role of the presynaptic Ca^{2+} stores, our data provide surprisingly little support for the role of the postsynaptic Ca^{2+} stores in AD-mediated dysfunction. Whereas previous in vitro data obtained in hippocampal and cortical tissue slices as well as primary cell cultures (23, 33, 48–51) have shown a strong (more than 200–300%) enhancement of the amplitude of somatic and dendritic caffeine as well as NMDA-evoked Ca^{2+} transients in AD mice, according to our in vivo data, the contribution of intracellular Ca^{2+} stores to somatic Ca^{2+} transients is minor. Although responses induced in layer 2/3 neurons by the RyR agonist caffeine were somewhat longer in AD mice, we did not observe any significant difference in the amplitudes of caffeine-induced Ca^{2+} transients between AD and WT mice. The largest differences were found in hyperactive cells of AD mice, in which T-half and tau, but not the amplitude or area under the caffeine-induced Ca^{2+} transient, were some 30–50% larger compared with the corresponding parameters measured in WT mice. Moreover,

NMDA-induced somatic Ca^{2+} transients in AD mice did not show any store-operated component.

Consistent with the somatic in vivo data, emptying intracellular Ca^{2+} stores in PS45 mice modulated synaptically evoked dendritic Ca^{2+} transients in hyperactive cells only. As we did not observe any differences in the amplitudes of dendritic Ca^{2+} transients between PS45 and WT mice in the absence of CPA, it cannot be excluded that the differences observed under CPA application reflect STIM1-dependent mechanisms similar to those described above for axonal boutons. Moreover, we did not observe any store contribution to dendritic Ca^{2+} transients in normal cells. This finding is in stark contrast to in vitro data showing a markedly reduced CICR threshold in synaptic compartments, such that basal synaptic stimulation is able to evoke greatly elevated dendritic Ca^{2+} transients in predepositing 4- to 6-wk-old AD mice (33). The mechanisms underlying such pronounced differences between former in vitro and present in vivo data remain unclear. They may be due to a different filling state of the stores caused by a reduced level of synaptic inhibition in tissue slices or due to the contribution of age-related factors not accounted for in in vitro experiments using juvenile/young adult animals. The level of RyRs, for example, was shown to be high in $PS1_{L286V}$ and 3xTg-AD mice at 6 wk of age, to be normal at 6 mo, and to increase again by 18 mo of age (52).

Working with hippocampal cell cultures, Sun et al. (53) have recently shown a significant reduction in the fraction of mushroom spines in neurons from $PS1_{M146V}$ mutant mice caused by the ER Ca^{2+} overload-mediated compensatory down-regulation of STIM2 protein and inhibition of neuronal store-operated Ca^{2+} influx. In contrast, in vivo data of Jung et al. (54) reported an increase of spine density in $PS1_{A246E}$-overexpressing mice. The reason for these opposing findings is unclear, as both above-mentioned mutations, along with the G384A mutation studied here, are supposed to diminish the ER leak channel function (55). Our dendritic data suggest that in vivo, the ER Ca^{2+} store-mediated destabilization of spines, if any, is likely to occur in hyperactive cells only. Alternatively, dendritic spines in hyperactive cells might be destabilized due to an increase in the open probability of NMDA receptors, leading to dendritic Ca^{2+} elevations and a concomitant activation of Ca^{2+}-dependent phosphatase calcineurin (56). Collectively, our in vivo data suggest that, on the postsynaptic side, only hyperactive neurons are susceptible to PS-mediated dysfunction.

Taken together, our data show that neuronal hyperactivity is a functional hallmark of the aging as well as the amyloid-depositing brain. However, the mechanisms underlying the hyperactivity differ. In mouse models of AD harboring FAD-related mutations in PS1, it is initiated presynaptically and is largely due to malfunction of the presynaptic intracellular Ca^{2+} stores. A single allele of mutated PS1 is sufficient to cause profound neuronal hyperactivity, but in amyloid-depositing mice, it might be further potentiated by soluble amyloid β species (15, 20) or activated neuroglia (57). At the same time, accumulation of amyloid β species may also cause neuronal silencing (58, 59), creating an uneven distribution of hyperactive cells throughout the brain (14, 15). The profound neuronal hyperactivity likely enhances activity-dependent generation and release of amyloid β and tau as well as formation of senile plaques (9, 56, 60, 61), thus explaining how a single mutation in the presenilin gene can lead to full-blown AD. On the postsynaptic side, neuronal hyperactivity causes more frequent openings of NMDA receptors, likely modulating NMDA receptor-dependent synaptic plasticity; potentiating NMDA-induced activation of calcineurin, caspase-3, and NO synthase (23, 56, 62); and causing an NO-mediated boosting of glutamatergic transmission (62). Together, these events build up a vicious cycle causing increasingly more hyperactivity, more aberrant neurotransmitter release, and synaptic and Ca^{2+} dyshomeostasis.

Materials and Methods

Detailed methods are provided in *SI Materials and Methods*.

Mice. All experiments were approved by the Regierungspraesidium Tuebingen, state government of Baden-Württemberg, Germany.

Virally Induced GCaMP6 Expression. A recombinant AAV was used to induce the expression of GCaMP6f in cortical neurons of the motor or barrel cortex. Axonal Ca^{2+} signals were analyzed 14 d after virus injection.

Acute Craniotomy and in Vivo Imaging. Surgery and labeling of neurons using the multicell bolus loading technique were performed as described elsewhere (25, 26). For single-cell electroporation, used for the analysis of dendritic Ca^{2+} signals, we adopted the protocol described by Nevian and Helmchen (63). In vivo imaging was performed with a custom-built two-photon microscope coupled to a mode-locked Ti-sapphire laser operating at a wavelength of 710–990 nm and a water immersion objective (40×, 0.8 N.A.; Nikon).

Drug Application. Drugs were applied either locally 30–40 μm away from the cells of interest using the pressure application technique or topically in the solution perfusing the recording chamber.

Immunohistochemistry. Sagittal cryoslices of the brain were labeled using antibodies against Iba-1 and CD68 as well as Thioflavin-S using standard techniques.

Quantification and Statistical Analysis. If not otherwise indicated, results show the median ± interquartile range. Depending on the distribution of the data in the dataset, differences were assessed using the Kolmogorov–Smirnov test, Student's *t* test, one-way ANOVA, two-way repeated measures ANOVA, or Friedman's test in conjunction with an appropriate post hoc test, as indicated in the figure legends. *P* values <0.05 were considered statistically significant.

ACKNOWLEDGMENTS. We thank E. Zirdum, A. Weible, G. Heck, and K. Schoentag for technical assistance as well as Ya. Okhrin and P. Martus for comments on the manuscript. We thank M. Jucker and J. Odenthal for providing APP_{swe} mice. The PS45 mice were originally obtained from M. Staufenbiel. This work was supported by Alzheimer Forschung Initiative e.V. Grant 14812 and VolkswagenStiftung Grant 90233 (both to O.G.) as well as *f*ortüne Grant 2200 (to B.B.).

1. Shen J, Kelleher RJ, 3rd (2007) The presenilin hypothesis of Alzheimer's disease: Evidence for a loss-of-function pathogenic mechanism. *Proc Natl Acad Sci USA* 104: 403–409.
2. Popugaeva E, Bezprozvanny I (2013) Role of endoplasmic reticulum Ca^{2+} signaling in the pathogenesis of Alzheimer disease. *Front Mol Neurosci* 6:29.
3. Zhang C, et al. (2009) Presenilins are essential for regulating neurotransmitter release. *Nature* 460:632–636.
4. Bezprozvanny I, Mattson MP (2008) Neuronal calcium mishandling and the pathogenesis of Alzheimer's disease. *Trends Neurosci* 31:454–463.
5. Hermes M, Eichhoff G, Garaschuk O (2010) Intracellular calcium signalling in Alzheimer's disease. *J Cell Mol Med* 14:30–41.
6. Chakroborty S, Stutzmann GE (2014) Calcium channelopathies and Alzheimer's disease: Insight into therapeutic success and failures. *Eur J Pharmacol* 739:83–95.
7. Haberman RP, Branch A, Gallagher M (2017) Targeting neural hyperactivity as a treatment to stem progression of late-onset Alzheimer's disease. *Neurotherapeutics* 14:662–676.
8. Palop JJ, Chin J, Mucke L (2006) A network dysfunction perspective on neurodegenerative diseases. *Nature* 443:768–773.
9. Palop JJ, Mucke L (2016) Network abnormalities and interneuron dysfunction in Alzheimer disease. *Nat Rev Neurosci* 17:777–792.
10. Palop JJ, Mucke L (2009) Epilepsy and cognitive impairments in Alzheimer disease. *Arch Neurol* 66:435–440.
11. Vossel KA, et al. (2016) Incidence and impact of subclinical epileptiform activity in Alzheimer's disease. *Ann Neurol* 80:858–870.
12. Bakker A, et al. (2012) Reduction of hippocampal hyperactivity improves cognition in amnestic mild cognitive impairment. *Neuron* 74:467–474.
13. Palop JJ, et al. (2007) Aberrant excitatory neuronal activity and compensatory remodeling of inhibitory hippocampal circuits in mouse models of Alzheimer's disease. *Neuron* 55:697–711.
14. Busche MA, et al. (2008) Clusters of hyperactive neurons near amyloid plaques in a mouse model of Alzheimer's disease. *Science* 321:1686–1689.
15. Busche MA, et al. (2012) Critical role of soluble amyloid-β for early hippocampal hyperactivity in a mouse model of Alzheimer's disease. *Proc Natl Acad Sci USA* 109:8740–8745.
16. Maier FC, et al. (2014) Longitudinal PET-MRI reveals β-amyloid deposition and rCBF dynamics and connects vascular amyloidosis to quantitative loss of perfusion. *Nat Med* 20:1485–1492.

17. Šišková Z, et al. (2014) Dendritic structural degeneration is functionally linked to cellular hyperexcitability in a mouse model of Alzheimer's disease. *Neuron* 84: 1023–1033.
18. Minkeviciene R, et al. (2009) Amyloid beta-induced neuronal hyperexcitability triggers progressive epilepsy. *J Neurosci* 29:3453–3462.
19. Verret L, et al. (2012) Inhibitory interneuron deficit links altered network activity and cognitive dysfunction in Alzheimer model. *Cell* 149:708–721.
20. Keskin AD, et al. (2017) BACE inhibition-dependent repair of Alzheimer's pathophysiology. *Proc Natl Acad Sci USA* 114:8631–8636.
21. Llano I, et al. (2000) Presynaptic calcium stores underlie large-amplitude miniature IPSCs and spontaneous calcium transients. *Nat Neurosci* 3:1256–1265.
22. Shimizu H, et al. (2008) Use-dependent amplification of presynaptic Ca^{2+} signaling by axonal ryanodine receptors at the hippocampal mossy fiber synapse. *Proc Natl Acad Sci USA* 105:11998–12003.
23. Chakroborty S, et al. (2012) Early presynaptic and postsynaptic calcium signaling abnormalities mask underlying synaptic depression in presymptomatic Alzheimer's disease mice. *J Neurosci* 32:8341–8353.
24. de Juan-Sanz J, et al. (2017) Axonal endoplasmic reticulum Ca^{2+} content controls release probability in CNS nerve terminals. *Neuron* 93:867–881.e6.
25. Stosiek C, Garaschuk O, Holthoff K, Konnerth A (2003) In vivo two-photon calcium imaging of neuronal networks. *Proc Natl Acad Sci USA* 100:7319–7324.
26. Garaschuk O, Milos RI, Konnerth A (2006) Targeted bulk-loading of fluorescent indicators for two-photon brain imaging in vivo. *Nat Protoc* 1:380–386.
27. Garaschuk O (2013) Imaging microcircuit function in healthy and diseased brain. *Exp Neurol* 242:41–49.
28. Davalos D, et al. (2005) ATP mediates rapid microglial response to local brain injury in vivo. *Nat Neurosci* 8:752–758.
29. Garaschuk O, et al. (2006) Optical monitoring of brain function in vivo: From neurons to networks. *Pflugers Arch* 453:385–396.
30. Garaschuk O, Yaari Y, Konnerth A (1997) Release and sequestration of calcium by ryanodine-sensitive stores in rat hippocampal neurones. *J Physiol* 502:13–30.
31. Shmigol A, Svichar N, Kostyuk P, Verkhratsky A (1996) Gradual caffeine-induced Ca^{2+} release in mouse dorsal root ganglion neurons is controlled by cytoplasmic and luminal Ca^{2+}. *Neuroscience* 73:1061–1067.
32. Koizumi S, Lipp P, Berridge MJ, Bootman MD (1999) Regulation of ryanodine receptor opening by lumenal Ca($^{2+}$) underlies quantal Ca($^{2+}$) release in PC12 cells. *J Biol Chem* 274:33327–33333.
33. Goussakov I, Miller MB, Stutzmann GE (2010) NMDA-mediated Ca($^{2+}$) influx drives aberrant ryanodine receptor activation in dendrites of young Alzheimer's disease mice. *J Neurosci* 30:12128–12137.
34. Rodgers KM, et al. (2009) The cortical innate immune response increases local neuronal excitability leading to seizures. *Brain* 132:2478–2486.
35. Sturchler-Pierrat C, et al. (1997) Two amyloid precursor protein transgenic mouse models with Alzheimer disease-like pathology. *Proc Natl Acad Sci USA* 94: 13287–13292.
36. Hessler NA, Shirke AM, Malinow R (1993) The probability of transmitter release at a mammalian central synapse. *Nature* 366:569–572.
37. Neher E, Sakaba T (2008) Multiple roles of calcium ions in the regulation of neurotransmitter release. *Neuron* 59:861–872.
38. Hooks BM, et al. (2013) Organization of cortical and thalamic input to pyramidal neurons in mouse motor cortex. *J Neurosci* 33:748–760.
39. Aronoff R, Petersen CC (2008) Layer, column and cell-type specific genetic manipulation in mouse barrel cortex. *Front Neurosci* 2:64–71.
40. Jia H, Rochefort NL, Chen X, Konnerth A (2010) Dendritic organization of sensory input to cortical neurons in vivo. *Nature* 464:1307–1312.
41. Smith SL, Smith IT, Branco T, Häusser M (2013) Dendritic spikes enhance stimulus selectivity in cortical neurons in vivo. *Nature* 503:115–120.
42. Flurkey K, Currer JM, Harrison DE (2007) The mouse in aging research. *The Mouse in Biomedical Research*, American College Laboratory Animal Medicine, eds Fox JG, et al. (Elsevier, Burlington, MA), pp 637–672.
43. Haberman RP, Koh MT, Gallagher M (2017) Heightened cortical excitability in aged rodents with memory impairment. *Neurobiol Aging* 54:144–151.
44. Simkin D, et al. (2015) Aging-related hyperexcitability in CA3 pyramidal neurons is mediated by enhanced A-type K^+ channel function and expression. *J Neurosci* 35: 13206–13218.
45. Grienberger C, et al. (2012) Staged decline of neuronal function in vivo in an animal model of Alzheimer's disease. *Nat Commun* 3:774.
46. Sanchez PE, et al. (2012) Levetiracetam suppresses neuronal network dysfunction and reverses synaptic and cognitive deficits in an Alzheimer's disease model. *Proc Natl Acad Sci USA* 109:E2895–E2903.
47. Lynch BA, et al. (2004) The synaptic vesicle protein SV2A is the binding site for the antiepileptic drug levetiracetam. *Proc Natl Acad Sci USA* 101:9861–9866.
48. Chakroborty S, et al. (2012) Stabilizing ER Ca^{2+} channel function as an early preventative strategy for Alzheimer's disease. *PLoS One* 7:e52056.
49. Chakroborty S, Goussakov I, Miller MB, Stutzmann GE (2009) Deviant ryanodine receptor-mediated calcium release resets synaptic homeostasis in presymptomatic 3xTg-AD mice. *J Neurosci* 29:9458–9470.
50. Schneider I, et al. (2001) Mutant presenilins disturb neuronal calcium homeostasis in the brain of transgenic mice, decreasing the threshold for excitotoxicity and facilitating long-term potentiation. *J Biol Chem* 276:11539–11544.
51. Zhang H, Sun S, Herreman A, De Strooper B, Bezprozvanny I (2010) Role of presenilins in neuronal calcium homeostasis. *J Neurosci* 30:8566–8580.
52. Stutzmann GE, et al. (2006) Enhanced ryanodine receptor recruitment contributes to Ca^{2+} disruptions in young, adult, and aged Alzheimer's disease mice. *J Neurosci* 26: 5180–5189.
53. Sun S, et al. (2014) Reduced synaptic STIM2 expression and impaired store-operated calcium entry cause destabilization of mature spines in mutant presenilin mice. *Neuron* 82:79–93.
54. Jung CKE, Fuhrmann M, Honarnejad K, Van Leuven F, Herms J (2011) Role of presenilin 1 in structural plasticity of cortical dendritic spines in vivo. *J Neurochem* 119: 1064–1073.
55. Nelson O, et al. (2007) Familial Alzheimer disease-linked mutations specifically disrupt Ca^{2+} leak function of presenilin 1. *J Clin Invest* 117:1230–1239.
56. Spires-Jones TL, Hyman BT (2014) The intersection of amyloid beta and tau at synapses in Alzheimer's disease. *Neuron* 82:756–771.
57. Brawek B, Garaschuk O (2014) Network-wide dysregulation of calcium homeostasis in Alzheimer's disease. *Cell Tissue Res* 357:427–438.
58. Selkoe DJ (2002) Alzheimer's disease is a synaptic failure. *Science* 298:789–791.
59. Haass C, Selkoe DJ (2007) Soluble protein oligomers in neurodegeneration: Lessons from the Alzheimer's amyloid beta-peptide. *Nat Rev Mol Cell Biol* 8:101–112.
60. Cirrito JR, et al. (2008) Endocytosis is required for synaptic activity-dependent release of amyloid-beta in vivo. *Neuron* 58:42–51.
61. Yamada K, et al. (2014) Neuronal activity regulates extracellular tau in vivo. *J Exp Med* 211:387–393.
62. Chakroborty S, Kim J, Schneider C, West AR, Stutzmann GE (2015) Nitric oxide signaling is recruited as a compensatory mechanism for sustaining synaptic plasticity in Alzheimer's disease mice. *J Neurosci* 35:6893–6902.
63. Nevian T, Helmchen F (2007) Calcium indicator loading of neurons using single-cell electroporation. *Pflugers Arch* 454:675–688.
64. Eichhoff G, Brawek B, Garaschuk O (2011) Microglial calcium signal acts as a rapid sensor of single neuron damage in vivo. *Biochim Biophys Acta* 1813:1014–1024.
65. Stettler DD, Yamahachi H, Li W, Denk W, Gilbert CD (2006) Axons and synaptic boutons are highly dynamic in adult visual cortex. *Neuron* 49:877–887.
66. De Paola V, et al. (2006) Cell type-specific structural plasticity of axonal branches and boutons in the adult neocortex. *Neuron* 49:861–875.